Article

Structure and Magnetism of Dinuclear Copper(II) Metallacyclophanes with Oligoacenebis(oxamate) Bridging Ligands: Theoretical Predictions on Wirelike Magnetic Coupling

Emilio Pardo, Rosa Carrasco, Rafael Ruiz-Garca, Miguel Julve, Francesc Lloret, M. Carmen Muoz, Yves Journaux, Eliseo Ruiz, and Joan Cano

J. Am. Chem. Soc., **2008**, 130 (2), 576-585 • DOI: 10.1021/ja0747066

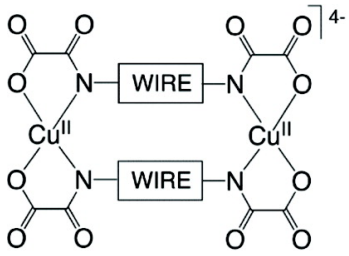

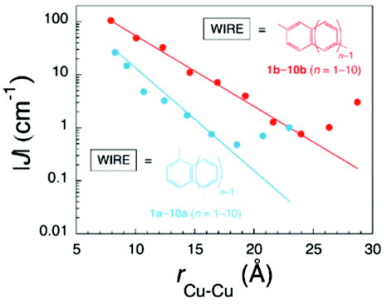

More About This Article

Additional resources and features associated with this article are available within the HTML version:

- Supporting Information
- Links to the 1 articles that cite this article, as of the time of this article download
- Access to high resolution figures
- Links to articles and content related to this article
- Copyright permission to reproduce figures and/or text from this article

View the Full Text HTML

J|A|C|S
ARTICLES
Published on Web 12/20/2007

Structure and Magnetism of Dinuclear Copper(II) Metallacyclophanes with Oligoacenebis(oxamate) Bridging Ligands: Theoretical Predictions on Wirelike Magnetic Coupling

Emilio Pardo,[†] Rosa Carrasco,[#] Rafael Ruiz-García,*[,‡,§] Miguel Julve,[†] Francesc Lloret,*[,†] M. Carmen Muñoz,[⊥] Yves Journaux,*[,∥] Eliseo Ruiz,[#] and Joan Cano*[,#,○]

Departament de Química Inorgànica and Departament de Química Orgànica, Instituto de Ciencia Molecular (ICMOL), and Fundació General de la Universitat de València (FGUV), Universitat de València, Paterna, València, E-46980 Spain, Departament de Física Aplicada, Universitat Politècnica de València, València, E-46071 Spain, Departament de Química Inorgànica, Institut de Química Teòrica i Computacional (IQTC) and Institut de Nanociència i Nanotecnologia (IN2UB), Universitat de Barcelona, Barcelona, E-08028 Spain, Institució Catalana de Recerca i Estudis Avançats (ICREA), and Laboratoire de Chimie Inorganique et Matériaux Moléculaires, Université Pierre et Marie Curie-Paris6, UMR 7071, Paris, F-75005 France

Received July 12, 2007; E-mail: rafael.ruiz@uv.es; francisco.lloret@uv.es; jour@ccr.jussieu.fr; joan.cano@qi.ub.es

Abstract: Self-assembly of the ligands *N*,*N*′-1,5-naphthalenebis(oxamate) (1,5-naba) and *N*,*N*′-2,6′-anthracenebis(oxamate) (2,6-anba) by Cu^{II} ions affords the two new dicopper(II) metallacyclophanes **2a** and **3b**, whereby the metal centers are connected by double naphthalene- and anthracenediamidate bridges with α,α' and β,β' substitution patterns, respectively. Despite the largely different intermetallic distances of 8.3 Å (**2a**) and 12.3 Å (**3b**), magnetic susceptibility measurements show a moderately strong antiferromagnetic coupling with rather similar *J* values in the range from −20.5 to −20.7 (**2a**) and from −21.2 to −23.0 (**3b**) cm^{-1} ($H = -J S_1 \cdot S_2$; $S_1 = S_2 = {}^1/_2$). Density functional theory calculations on the two series of dicopper(II) metallacyclophanes **1a**−**10a** and **1b**−**10b** with linear α,α'- and β,β'-disubstituted oligoacenediamidate bridges, respectively, confirm the better efficiency of the latter substitution pattern on long-range magnetic coupling. More importantly, they predict a unprecedented wirelike magnetic behavior for the longest members of the series with octacene through decacene spacers (*J* values up to +3.0 cm^{-1} for intermetallic distances reaching 28.8 Å).

1. Introduction

Polymetallic complexes with strong exchange interactions between distant metal centers across extended bridges are a major topic of molecular magnetism,[1] which exceeds its own field of research of magnetochemistry to include other domains of physics and biology.[2,3] The transport of electrons across relevant length scales either in nanometer-scale metal-based electronic devices[2] or in electron-carrier metalloproteins[3] are certainly noteworthy examples of long-distance metal−metal electronic coupling in artificial and natural systems, respectively. From a fundamental point of view, electron exchange and electron transfer are intimately related processes that rely on

[†] Departament de Química Inorgànica, ICMOL, Universitat de València.
[‡] Departament de Química Orgànica, ICMOL, Universitat de València.
[§] FGUV, Universitat de València.
[⊥] Departament de Física Aplicada, Universitat Politècnica de València.
[∥] Laboratoire de Chimie Inorganique et Matériaux Moléculaires, Université Pierre et Marie Curie-Paris6, UMR 7071.
[#] Departament de Química Inorgànica, IQTC and IN2UB, Universitat de Barcelona.
[○] ICREA.

(1) (a) Kahn, O. *Molecular Magnetism*; VCH Publishers: New York, 1993. (b) Hay, J. P.; Thibeault, J. C.; Hoffmann, R. *J. Am. Chem. Soc.* **1975**, *97*, 4884. (c) Kahn, O. *Angew. Chem., Int. Ed. Engl.* **1985**, *24*, 834. (d) *Magneto-Structural Correlations in Exchange Coupled Systems*; Willett, R. D., Gatteschi, D., Kahn, O., Eds.; Reidel: Dordrecht, The Netherlands, 1985.

(2) (a) *Molecular Electronics*; Jorner, J., Ratner, M., Eds.; Blackwell Science: Oxford, 1997. (b) *Molecular Electronics: Science and Technology*; Aviram, A., Ratner, M., Eds.; Annals of the New York Academy of Sciences: New York, 1998. (c) Joachim, C.; Gimzewski, J. K.; Aviram, A. *Nature* **2000**, *408*, 541. (d) Park, J.; Pasupathy, A. N.; Goldsmith, J. I.; Chang, C.; Yaish, Y.; Petta, J. R.; Rinkoski, M.; Sethna, J. P.; Abruña, H. D.; McEuen, P. L.; Ralph, D. C. *Nature* **2002**, *417*, 722. (e) Liang, W.; Shores, M. P.; Bockrath, M.; Long, J. R.; Park, H. *Nature* **2002**, *417*, 725. (f) Smith, R. H. M.; Noat, Y.; Untiedt, C.; Lang, N. D.; Van Hemert, M. C.; Van Rultenbeek, J. M. *Nature* **2002**, *419*, 906. (g) Ng, M. K.; Lee, D. C.; Yu, L. *J. Am. Chem. Soc.* **2002**, *124*, 11862. (h) Carrol, R. L.; Gorman, C. B. *Angew. Chem., Int. Ed.* **2002**, *41*, 4378.

(3) (a) Bowler, B. E.; Raphael, A. L.; Gray, H. B. *Prog. Inorg. Chem.* **1990**, *38*, 259. (b) *Electron Transfer Reactions in Metalloproteins*; Sigel, H., Ed.; Metal Ions in Biological Systems, Vol. 27; Marcel Dekker: New York, 1991. (c) Beratan, D. N.; Onuchic, J. N.; Winkler, J. R.; Gray, H. B. *Science* **1992**, *258*, 1740. (d) Pelletier, H.; Kraut, J. *Science* **1992**, *258*, 1748. (e) Solomon, E. I.; Lowery, M. D. *Science* **1993**, *259*, 1575. (f) Lippard, S. J.; Berg, J. M. *Principles of Bioinorganic Chemistry*; University Science Books: Mill Valley, California, 1994 and references therein. (g) Gamelin, D. R.; Randall, D. W.; Hay, M. T.; Houser, R. P.; Mulder, T. C.; Canters, G. W.; De Vries, S.; Tolman, W. B.; Lu, Y.; Solomon, E. I. *J. Am. Chem. Soc.* **1998**, *120*, 5246.

 10.1021/ja0747066 CCC: $40.75

the transmission of spin- and charge-based electronic effects, respectively.[4] Intervalence electron transfer through extended π-conjugated aromatic bridges has been achieved in dinuclear mixed-valence complexes with intermetallic distances reaching 25 Å.[5] However, similar examples of long-range magnetic coupling in dinuclear exchange-coupled complexes are still unknown.[6] The design and synthesis of novel bridging ligands which can act as effective molecular wires to transmit spin coupling effects over long distances is thus a major achievement in the field, which requires both a skilful organic synthesis and a deep understanding of the electron exchange mechanism. With the advent of calculations based on the density functional theory (DFT) combined with the broken-symmetry (BS) approach, it has been possible not only to accurately reproduce but also to really predict the magnetic properties of dinuclear complexes expressed in terms of the exchange coupling constant (J) introduced by the phenomenological spin Hamiltonian $H = -J\, S_1 \cdot S_2$.[7]

Dinuclear copper(II) metallacyclophanes are indeed ideal model systems for the study of the electron exchange mechanism between paramagnetic metal centers containing one unpaired electron ($S_1 = S_2 = {}^1/_2$) through extended π-conjugated aromatic bridges in a discrete metallacyclic entity, but however they have received limited attention.[8] The variation of the ligand spacer may control both the overall structure and the magnetic behavior of the metallacyclophane complex, and the influence of different factors such as the topology and conformation of the bridging ligand can then be investigated in a systematic way. In particular, the problem of long-range magnetic coupling in dinuclear copper(II) metallacyclophanes has been addressed by several research teams through the use of diverse coordinating group substituted aromatic bridging ligands, either acyclic or macrocyclic, with more or less satisfactory results (Table S1, Supporting Information).[9−11] There is no simple correlation between the magnetic coupling and the intermetallic distance for the reported examples of structurally characterized dicopper(II) metallacyclophanes with amine-,[9] imine-,[10] and amide-based[11] aromatic bridges (Figure 1). In general, for those dicopper(II) metallaazacyclophanes with extended aromatic spacers of comparable Cu−Cu distances, the magnitude of the magnetic coupling in the amide series is more than 4-fold greater than the largest one in the amine and imine series. With one notable exception,[10d] weak antiferromagnetic couplings ($-J$ values smaller than 2.2 cm^{-1}) have been observed for the dicopper(II) metallacyclophanes with amine- and imine-based aromatic bridges possessing rather long intermetal distances (r values larger than 7.0 Å) (Table S1, entries 1−8).[9,10b,c,e] On the contrary, Inoue *et al.* have reported moderate to strong antiferromagnetic couplings in the related dicopper(II) metallacyclophanes with amide-based aromatic bridges ($-J$ values up to 105 cm^{-1}) (Table S1, entries 9−11).[11d] It appears that the exchange interaction between the Cu^{II} ions involves predominantly π-type orbital pathways in the amide series, whereas it is mainly transmitted through the σ-electron system of the aromatic bridge in the amine and imine series, with little or no contribution from the π-electron system.

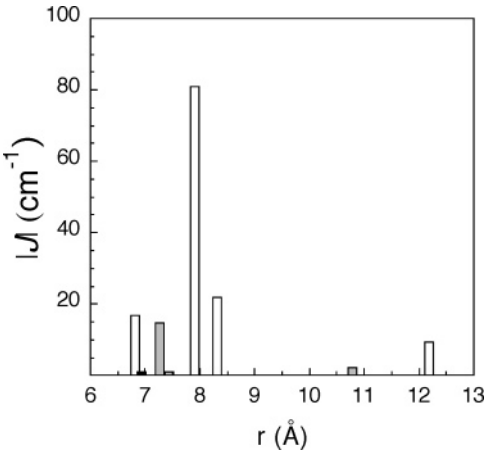

Figure 1. Dependence of the magnetic coupling with the intermetallic distance for dinuclear copper(II) metallaazacyclophanes with aromatic bridging ligands: amine (black), imine (gray), and amide (white) series (data from Table S1).

In this context, we recently reported on the structure and magnetism of a unique series of dinuclear copper(II) metallacyclophanes with oligophenylenebis(oxamate) ligands.[12] By using this kind of bis-bidentate dinucleating ligands consisting of two oxamate units as metal binding sites interconnected by a more or less rigid oligophenylene spacer, discrete double-stranded dicopper(II) metallacyclic complexes may be prepared. These bridging ligands are designed in such a way that the two coplanar aromatic groups stabilized by π-stacking interactions are perpendicular with the basal planes of the square-planar Cu^{II}

(4) (a) Creutz, C. *Prog. Inorg. Chem.* **1983**, *30*, 1. (b) Blondin, G.; Girerd, J. J. *Chem. Rev.* **1990**, *90*, 1359. (c) Crutchley, R. J. *Adv. Inorg. Chem.* **1994**, *41*, 273. (d) Brunschwig, B. S.; Sutin, N. *Coord. Chem. Rev.* **1999**, *187*, 233.
(5) (a) McCleverty, J. A.; Ward, M. D. *Acc. Chem. Res.* **1998**, *36*, 3447. (b) Launay, J. P. *Chem. Soc. Rev.* **2001**, *30*, 386.
(6) (a) Bürger, K. S.; Chaudhuri, P.; Wieghardt, K.; Nuber, B. *Chem.—Eur. J.* **1995**, *1*, 583. (b) Cargill-Thompson, A. M. W.; Gatteschi, D.; McCleverty, J. A.; Navas, J. A.; Rentschler, E.; Ward, M. D. *Inorg. Chem.* **1996**, *35*, 2701. (c) Ung, V. A.; Cargill-Thompson, A. M. W.; Bardwell, D. A.; Gatteschi, D.; Jeffery, J. C.; McCleverty, J. A.; Totti, F.; Ward, M. D. *Inorg. Chem.* **1997**, *36*, 3447. (d) Ung, V. A.; Couchman, S. M.; Jeffery, J. C.; McCleverty, J. A.; Ward, M. D.; Totti, F.; Gatteschi, D. *Inorg. Chem.* **1999**, *38*, 365. (e) Bayly, S.; McCleverty, J. A.; Ward, M. D.; Gatteschi, D.; Totti, F. *Inorg. Chem.* **2000**, *39*, 1288. (f) Fabre, M.; Bonvoisin, J. *J. Am. Chem. Soc.* **2007**, *129*, 1434.
(7) (a) Bencini, A.; Gatteschi, D.; Totti, F.; Nieto-Sanz, D.; Mc Cleverty, J. A.; Ward, M. D. *J. Phys. Chem. A* **1998**, *102*, 10545. (b) Ruiz, E.; Rodríguez-Fortea, A.; Alvarez, S. *Inorg. Chem.* **2003**, *42*, 4881. (c) Paital, A. R.; Mitra, T.; Ray, D.; Wong, W. T.; Ribas-Ariño, J.; Novoa, J. J.; Ribas, J.; Aromí, G. *Chem. Commun.* **2005**, 5172. (d) Nunzi, F.; Ruiz, E.; Cano, J.; Alvarez, S. *J. Phys. Chem. C* **2007**, *111*, 618.
(8) Swiegers, G. F.; Malefetse, T. J. *Chem. Rev.* **2000**, *100*, 3483.
(9) (a) Mederos, A.; Gili, P.; Domínguez, S.; Benítez, A., Palacios, M. S.; Hernández-Padilla, M.; Martín-Zarza, P.; Rodríguez, M. L.; Ruiz-Pérez, C.; Lahoz, F. J.; Oro, L. A.; Brito, F.; Arrieta, J. M.; Vlassi, M.; Germain, G. *J. Chem. Soc., Dalton Trans.* **1990**, 1477. (b) Domínguez, S.; Mederos, A.; Gili, P.; Rancel, A.; Rivero, A. E.; Brito, F.; Lloret, F.; Solans, X.; Ruiz-Pérez, C.; Rodríguez, M. L.; Brito, I. *Inorg. Chim. Acta* **1997**, *255*, 367.
(10) (a) Bear, C. A.; Waters, J. M.; Waters, T. N. *J. Chem. Soc. A* **1970**, *17*, 2494. (b) Jeter, D. Y.; Hatfield, W. E. *Inorg. Chim. Acta* **1972**, *6*, 440. (c) Hernández-Molina, R.; Mederos, A.; Gili, P.; Domínguez, S.; Lloret, F.; Cano, J.; Julve, M.; Ruiz-Pérez, C.; Solans, X. *J. Chem. Soc., Dalton Trans.* **1997**, 4327. (d) Paital, A. R.; Mitra, T.; Ray, D.; Wong, W. T.; Ribas-Ariño, J.; Novoa, J. J.; Ribas, J.; Aromí, G. *Chem. Commun.* **2005**, 5172. (e) Paital, A. R.; Wu, A. Q.; Guo, G. G.; Aromí, G.; Ribas-Ariño, J.; Ray, D. *Inorg. Chem.* **2007**, *46*, 2947. (f) Vázquez, M.; Taglietti, A.; Gatteschi, D.; Sorace, L.; Sangregorio, C.; González, A. M.; Maneiro, M.; Pedrido, R. M.; Bermejo, M. R. *Chem. Commun.* **2003**, 1840.
(11) (a) Inoue, M. B.; Velázquez, E. F.; Medrano, F.; Ochoa, K. L.; Gálvez, J. C.; Inoue, M.; Fernando, Q. *Inorg. Chem.* **1998**, *37*, 4070. (b) Inoue, M. B.; Muñoz, I. C.; Machi, L.; Inoue, M.; Fernando, Q. *Inorg. Chim. Acta* **2000**, *311*, 50. (c) Inoue, M. B.; Inoue, M.; Sugich-Miranda, R.; Machi, L.; Velázquez, E. F.; Fernando, Q. *Inorg. Chim. Acta* **2001**, *317*, 181. (d) Mosina, L. V.; Raitsimring, A. V.; Inoue, M. B.; Fernando, Q.; Inoue, M. *Appl. Magn. Reson.* **2001**, *20*, 249.
(12) (a) Fernández, I.; Ruiz, R.; Faus, J.; Julve, M.; Lloret, F.; Cano, J.; Ottenwaelder, X.; Journaux, Y.; Muñoz, M. C. *Angew. Chem., Int. Ed.* **2001**, *40*, 3039. (b) Pardo, E.; Faus, J.; Julve, M.; Lloret, F.; Muñoz, M. C.; Cano, J.; Ottenwaelder, X.; Journaux, Y.; Carrasco, R.; Blay, G.; Fernández, I.; Ruiz-García, R. *J. Am. Chem. Soc.* **2003**, *125*, 10770.

Scheme 1. Structural Formula of the Dinuclear Copper(II) Metallacyclophanes with α,α′- (**1a**−**10a**) and *β*,*β*′-disubstituted (**1b**−**10b**) Oligoacene Spacers

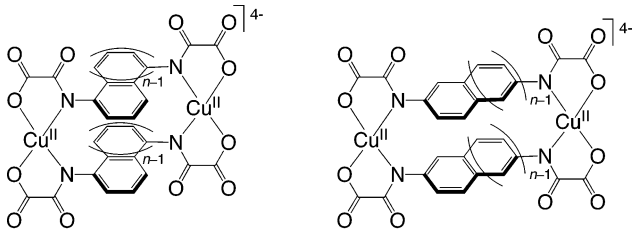

1a–**10a** (*n* = 1–10) **1b**–**10b** (*n* = 1–10)

ions, owing to their mutual steric repulsion when they are brought closer by metal coordination. This overall orthogonal conformation of the dicopper(II) metallacyclophane complex allowed for an evaluation of the efficiency of the *π*- versus *σ*-pathway across extended aromatic bridges for the propagation of the exchange interaction between the two unpaired electrons of each square-planar Cu^{II} ion. A moderate ferro- ($J = +16.8$ cm^{-1})[12a] to strong antiferromagnetic ($-J = 81-95$ cm^{-1})[12b] coupling has been observed for the parent members of this series with double *m*- and *p*-phenylenediamidate bridges, respectively (Table S1, entries 12−15). Both effects result from spin polarization of the extended *π*-conjugated bond system of the phenylene spacers with *meta*- and *para*-substitution patterns. Yet, the magnetic coupling decreases dramatically for the dicopper(II) metallacyclophane with double bi-*p*-phenylenediamidate bridges, which exhibits a moderate to weak antiferromagnetic coupling ($-J = 8.7-11.5$ cm^{-1}) (Table S1, entries 16−18).[12b] This has been supported by DFT calculations which predict an exponential decay of the magnetic coupling with the intermetallic distance when increasing the number of C−C single bonds in the oligo-*p*-phenylene spacers.[12b] These results have oriented our current research toward other dicopper(II) metallacyclophane molecules with greater *π*-conjugated aromatic spacers. In this respect, oligoacenes are very appealing candidates as molecular wires because of their unique electronic properties which have received much attention both experimentally and theoretically.[13,14]

In this paper, we present a combined experimental and theoretical study on a new family of dinuclear copper(II) metallacyclophanes with oligoacene spacers consisting of linearly fused benzenoid units, $-(C_{2+4n}H_{2+2n})-$ ($n = 1-10$), differently substituted at the carbon atoms of the terminal benzene rings, either α,α′- (**1a**−**10a**) or *β*,*β*′-disubstituted (**1b**−**10b**) (Scheme 1). We report here the synthesis, the physical and structural characterization, and the magnetic properties of the two novel dicopper(II) metallacyclophanes **2a** and **3b** with the ligands *N*,*N*′-1,5-naphthalenebis(oxamate) (1,5-naba) and *N*,*N*′-2,6′-anthracenebis(oxamate) (2,6-anba), respectively. Molecular and electronic structure DFT calculations on the two series of dicopper(II) metallacyclophanes **1a**−**10a** and **1b**−**10b** with linear α,α′- and *β*,*β*′-disubstituted oligoacenebis(oxamate) ligands, respectively, allow us to examine the role of the bridging ligand topology on long-range magnetic coupling. More importantly, the computational results show that oligoacenes would behave as molecular wires for the propagation of the exchange interaction between the unpaired electrons of the two Cu^{II} centers with intermetallic distances in the range 8−30 Å.

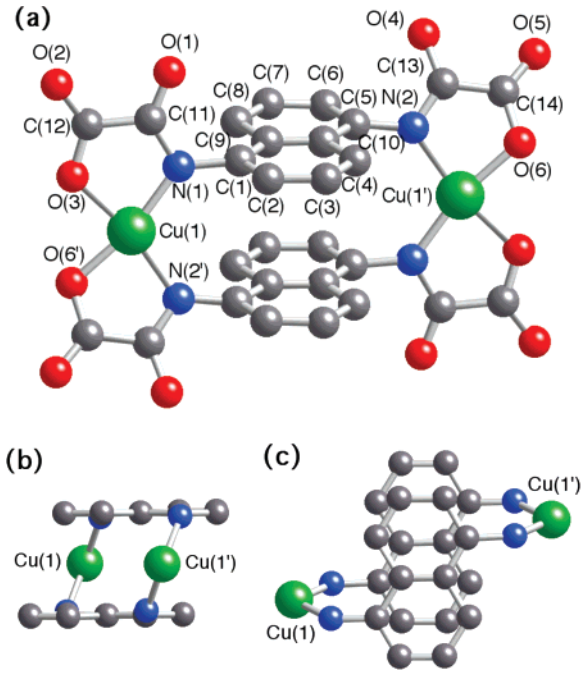

Figure 2. (a) Perspective view of the centrosymmetric anionic dicopper unit of $(Ph_4P)_4$**2a**·$8H_2O$ with the atom-numbering scheme (hydrogen atoms have been omitted for clarity) (symmetry code: (I) = − *x*, − *y*, − *z*). (b) Side and (c) top projection views of the dicoppertetraaza[3.3](1,5)-naphthalenophane metallacyclic core.

2. Results and Discussion

Syntheses of Ligands and Complexes. The proligands *N*,*N*′-1,5-naphthalenebis(oxamic acid) (H_4-1,5-naba) and *N*,*N*′-2,6′-anthracenebis(oxamic acid) (H_4-2,6-anba) were synthesized from the straightforward condensation of either 1,5-naphthalenediamine or 2,6-anthracenediamine, respectively, with ethyl oxalyl chloride ester (1:2 ratio) in THF in the presence of triethylamine, and they were isolated as the diethyl ester derivatives in very good yields (80−85%). The tetraanionic dinuclear copper(II) complexes, $[Cu_2(1,5\text{-naba})_2]^{4-}$ (**2a**) and $[Cu_2(2,6\text{-anba})_2]^{4-}$ (**3b**), were synthesized by reaction of the diethyl ester derivatives of H_4-1,5-naba and H_4-2,6-anba, respectively, with Cu^{II} nitrate salt (2:2 molar ratio) in basic H_2O/MeOH solution by using Li^I hydroxide as base. They were isolated as the lithium salts of formula Li_4**2a**·$12H_2O$ and Li_4**3b**·$12H_2O$ in moderate to good yields (40−60%), which after metathesis with Ph_4PCl in water gave the corresponding tetraphenylphosphonium salts of formula $(Ph_4P)_4$**2a**·$8H_2O$ and $(Ph_4P)_4$**3b**·$4H_2O$ in good yields (70−80%). The chemical identity of the ligands and the complexes was obtained from elemental analysis and from ^1H NMR and IR spectroscopies (see Experimental Section). The structure of $(Ph_4P)_4$**2a**·$8H_2O$ was unequivocally determined by single-crystal X-ray diffraction. Up to now, all our attempts to grow X-ray quality crystals of $(Ph_4P)_4$**3a**·$4H_2O$ were unsuccessful.

Description of the Structure. Single-crystal X-ray diffraction analysis of $(Ph_4P)_4$**2a**·$8H_2O$ confirmed the dicoppertetraaza[3.3]-(1,5)naphthalenophane metallacyclic core structure for the tetraanionic dinuclear complex **2a** (Figure 2). A summary of

(13) (a) Clar, E. *Polycyclic Hydrocarbons*; Academic Press: London, U.K., 1964; Vols. 1 and 2. (b) Geerts, Y.; Klärner, G.; Müllen, K. In *Electronic Materials: The Oligomer Approach*; Müllen, K., Klärner, G., Eds.; Wiley-VCH: Weinheim, Germany, 1998; p 48.
(14) (a) Bendikov, M.; Duong, H. M.; Starkey, K.; Houk, K. N.; Carter, E. A.; Wudl, F. *J. Am. Chem. Soc.* **2004**, *126*, 7416. (b) Norton, J. E.; Houk, K. N. *J. Am. Chem. Soc.* **2005**, *127*, 4162.

Table 1. Summary of Crystallographic Data for $(Ph_4P)_4$**2a**·$8H_2O$

formula	$C_{124}H_{108}Cu_2N_4O_{20}P_4$
M (g mol^{-1})	2225.1
crystal system	monoclinic
space group	$P2_1/n$
a (Å)	16.024(5)
b (Å)	24.939(3)
c (Å)	16.859(3)
β (deg)	113.376(19)
V (Å^3)	6184(2)
Z	2
ρ_{calc} (g cm^{-3})	1.195
μ (mm^{-1})	0.460
T (K)	293(2)
R^a [$I > 2\sigma(I)$]	0.0865
wR^b [$I > 2\sigma(I)$]	0.2170
S^c	1.11

[a] $R = \sum(|F_o| - |F_c|)/\sum|F_o|$. [b] $wR = [\sum w(|F_o| - |F_c|)^2/\sum w|F_o|^2]^{1/2}$. [c] $S = [\sum w(|F_o| - |F_c|)^2/(N_o - N_p)]^{1/2}$.

Table 2. Selected Bond Distances (Å) and Angles (deg) for $(Ph_4P)_4$**2a**·$8H_2O$[a,b]

Cu(1)−N(1)	1.946(12)	Cu(1)−N(2^I)	1.979(13)
Cu(1)−O(3)	1.923(11)	Cu(1)−O(6^I)	1.905(13)
N(1)−C(1)	1.469(17)	N(2)−C(5)	1.411(18)
C(1)−C(2)	1.426(19)	C(5)−C(6)	1.42(2)
C(2)−C(3)	1.366(18)	C(6)−C(7)	1.35(2)
C(3)−C(4)	1.371(19)	C(7)−C(8)	1.38(2)
C(4)−C(10)	1.48(2)	C(8)−C(9)	1.441(19)
C(9)−C(10)	1.348(17)		
N(1)−Cu(1)−N(2^I)	107.9(5)	N(1)−Cu(1)−O(3)	83.9(5)
N(1)−Cu(1)−O(6^I)	166.5(5)	N(2)−Cu(1)−O(3)	168.2(5)
N(2)−Cu(1)−O(6^I)	85.5(6)	O(3)−Cu(1)−O(6^I)	82.7(5)
Cu(1)−N(1)−C(1)	131.8(9)	Cu(1^I)−N(2)−C(5)	130.6(11)
N(1)−C(1)−C(2)	117.0(14)	N(2)−C(5)−C(6)	120.6(15)
N(1)−C(1)−C(9)	122.3(13)	N(2)−C(5)−C(10)	122.8(15)
C(2)−C(1)−C(9)	120.6(13)	C(6)−C(5)−C(10)	116.4(14)
C(1)−C(2)−C(3)	119.3(14)	C(5)−C(6)−C(7)	119.3(16)
C(2)−C(3)−C(4)	121.2(14)	C(6)−C(7)−C(8)	124.4(16)
C(3)−C(4)−C(10)	118.7(13)	C(7)−C(8)−C(9)	117.9(15)
C(4)−C(10)−C(5)	117.1(14)	C(8)−C(9)−C(1)	120.8(13)
C(4)−C(10)−C(9)	118.6(13)	C(8)−C(9)−C(10)	117.7(14)
C(5)−C(10)−C(9)	124.2(14)	C(1)−C(9)−C(10)	121.5(13)

[a] The estimated standard deviations are given in parentheses. [b] Symmetry code: (I) = $-x, -y, -z$.

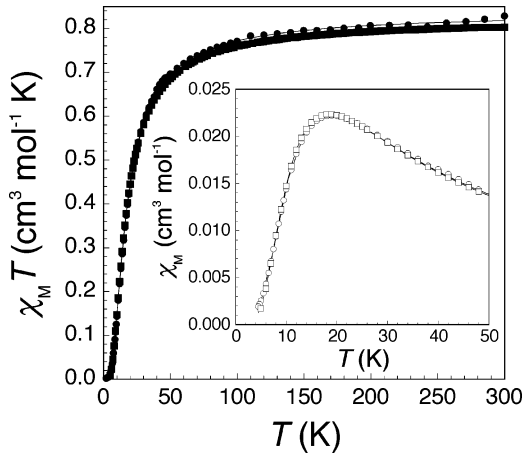

Figure 3. Temperature dependence of $\chi_M T$ for Li_4**2a**·$12H_2O$ (●) and $(Ph_4P)_4$**2a**·$8H_2O$ (■). The inset shows the maxima of χ_M for Li_4**2a**·$12H_2O$ (○) and $(Ph_4P)_4$**2a**·$8H_2O$ (□) in the low-temperature region. Solid lines correspond to the best fits (see text).

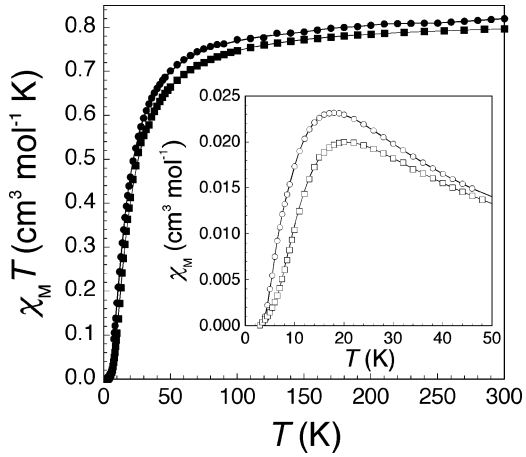

Figure 4. Temperature dependence of $\chi_M T$ for Li_4**3b**·$12H_2O$ (●) and $(Ph_4P)_4$**3b**·$4H_2O$ (■). The inset shows the maxima of χ_M for Li_4**3b**·$12H_2O$ (○) and $(Ph_4P)_4$**3b**·$4H_2O$ (□) in the low-temperature region. Solid lines correspond to the best fits (see text).

the crystallographic data are listed in Table 1. Selected bond lengths and angles are given in Table 2. In the crystal lattice, the centrosymmetric dinuclear copper(II) anions are well separated from each other by the bulky tetraphenylphosphonium cations and the hydrogen-bonded crystallization water molecules (Figure S1, Supporting Information). The intramolecular Cu(1)−Cu(1^I) distance (r) through the double 1,5-naphthalenediamidate bridge is 8.331(3) Å, whereas the shortest intermolecular Cu(1)−Cu(1^{II}) and Cu(1)−Cu(1^{III}) distances are 11.786(3) and 16.155(3) Å, respectively (symmetry codes: (I) = $-x, -y, -z$; (II) = $1 - x, -y, -z$; (III) = $-x, -y, 1 - z$).

The essentially square-planar environment of the copper atom is formed by two amidate-nitrogen and two carboxylate-oxygen atoms, CuN_2O_2, with an average Cu−N distance of 1.96 Å which is slightly longer than the average Cu−O distance of 1.91 Å. The N−Cu−O bite angles of 83.9(5)° and 85.5(6)° are close to 90°, whereas the N−Cu−N angle of 107.9(5)° is greater than the O−Cu−O angle of 82.7(5)° because of the $\pi-\pi$ repulsion interactions between the two bridging naphthalene groups. The naphthalene group is nearly planar, with a twist angle (τ) of 3(1)° between the two fused benzene rings. A small but nonnegligible bond alternation is observed in the benzene rings, with average long and short C−C distances of 1.44 and 1.39 Å, respectively. The C−C−C angles vary in the range 116.4(14)°−124.4(16)°, values which are close to that of 120° as expected for a sp^2 hybridization. As in the parent complex **1a**,[12b] the copper basal planes are not exactly oriented perpendicular to the aromatic naphthalene planes, but they form a dihedral angle (ϕ) of 75.3(5)° (Figure 2b). Deviations from an ideal C_{2h} symmetry may be originated from the favorable $\pi-\pi$ interactions in the parallel-displaced configuration of the naphthalene groups (Figure 2c). The average C−C distance of 3.46 Å between the two facing naphthalene groups connected by the two N−Cu−N linkages is slightly longer than the van der Waals contact.

Magnetic Properties. The magnetic properties of the lithium and tetraphenylphosphonium salts of complexes **2a** and **3b** in the form of χ_M and $\chi_M T$ versus T plots (χ_M being the molar magnetic susceptibility per dinuclear unit and T the temperature) are typical of antiferromagnetically coupled Cu^{II}_2 pairs (Figures 3 and 4). At room temperature, $\chi_M T$ is in the narrow range 0.80−0.83 cm^3 mol^{-1} K, values which are close to that expected for two magnetically noninteracting Cu^{II} ions ($\chi_M T$ = 0.83 cm^3 mol^{-1} K with g = 2.1). Upon cooling, $\chi_M T$ continuously

Table 3. Selected Magnetic Data for Complexes **2a** and **3b**

complex	J (cm^{-1})[a]	g[b]	R[c]
Li_4**2a**·12H_2O	−20.5	2.12	1.4×10^{-6}
$(Ph_4P)_4$**2a**·8H_2O	−20.7	2.10	1.1×10^{-6}
Li_4**3b**·12H_2O	−21.2	2.11	1.0×10^{-6}
$(Ph_4P)_4$**3b**·4H_2O	−23.0	2.10	1.1×10^{-6}

[a] Exchange coupling constant in the spin Hamiltonian $H = -JS_1 \cdot S_2$ ($S_1 = S_2 = {}^1/_2$). [b] Zeeman factor. [c] Agreement factor defined as $R = \sum[(\chi_M T)_{exp} - (\chi_M T)_{calcd}]^2/\sum[(\chi_M T)_{exp}]$.[2]

decreases and vanishes at ca. 4.0 K, whereas χ_M exhibits a characteristic maximum around 20 K which unambiguously indicates a diamagnetic singlet ($S = 0$) ground state (inset of Figures 3 and 4). The qualitatively similar magnetic behavior with variation in the countercation for both **2a** and **3b** demonstrates that the magnetic coupling is intramolecular in origin, the intermolecular interactions through the lithium ions, if any, being negligible.

A least-squares fit of the experimental data through the Bleaney−Bowers equation gave $J = -20.5$ cm^{-1} and $g = 2.12$ for Li_4**2a**·12H_2O, $J = -20.7$ cm^{-1} and $g = 2.10$ for $(Ph_4P)_4$**2a**·8H_2O, $J = -21.2$ cm^{-1} and $g = 2.11$ for Li_4**3b**·12H_2O, and $J = -23.0$ cm^{-1} and $g = 2.10$ for $(Ph_4P)_4$**3b**·4H_2O (Table 3). The theoretical curves reproduce perfectly well the experimental data (solid lines in Figures 3 and 4). Overall, the moderately strong antiferromagnetic coupling observed in these complexes indicates that the available π-type exchange pathways across the naphthalene (**2a**) and anthracene (**3b**) spacers are really effective in propagating an intramolecular exchange interaction between the unpaired electrons of each square-planar Cu^{II} ion. In this respect, two aspects deserve to be mentioned. First, the $-J$ values for the lithium and tetraphenylphosphonium salts of complex **2a** ($-J = 20.5-20.7$ cm^{-1}) are similar to that found in the only other reported example of dicopper(II) metallacyclophane with a double 1,5-naphthalenediamidate bridge ($-J = 22.0$ cm^{-1}) (Table S1, entry 10).[11d] Second, the comparable or even larger $-J$ values for the lithium and tetraphenylphosphonium salts of complex **3b** ($-J = 21.2-23.0$ cm^{-1}) are quite remarkable given the larger Cu−Cu separation through the double 2,6-anthracenediamidate bridge (see below). Interestingly, the related dicopper(II) metallacyclophane with a double bi-*p*-phenylenediamidate bridge, which has a similar intermetallic distance ($r = 12.2$ Å), exhibits a weak to moderate antiferromagnetic coupling ($-J = 8.7-11.5$ cm^{-1}) (Table S1, entries 16−18).[12b] This clearly evidences the greater efficiency of the oligoacene spacers compared to the oligo-*p*-phenylene ones in the transmission of the exchange interaction, as expected from their better π-conjugation. Once again, this fact illustrates the large influence of the nature of the extended π-conjugated aromatic spacer (substitution pattern, conformation, or presence of heteroatoms) on the magnetic coupling through π-type exchange pathways for this family of dicopper(II) amide-based metallacyclophanes (Table S1, entries 9−18).[11,12]

Energy Calculations: Distance Dependence of Magnetic Coupling. DFT energy calculations on the model complexes **2a** and **3b**, with ideal C_{2h} symmetry (see Computational Details), showed a ground singlet spin state lying well below the excited triplet spin state. For estimated intermetallic distances (r) of 8.3 (**2a**) and 12.3 Å (**3b**), the calculated values of the singlet−triplet energy gap ($\Delta E_{ST} = |J|$) are 26.0 (**2a**) and 32.2 cm^{-1} (**3b**) (Tables 4 and 5). These theoretical results agree with the experimental ones concerning the relative importance of the magnetic coupling in the lithium and tetraphenylphosphonium salts of complexes **2a** ($-J = 20.5-20.7$ cm^{-1}) and **3b** ($-J = 21.2-23.0$ cm^{-1}). The experimental $-J$ values are, however, somewhat smaller than the calculated ones likely due to the partial loss of orthogonality between the copper and aromatic planes ($\phi \neq 90°$) and/or the twisting of the aromatic groups ($\tau \neq 0°$).[12b]

Table 4. Selected Calculated Magnetostructural Data for Model Complexes **1a**−**10a**

complex	r (Å)[a]	J (cm^{-1})[b]	$\langle S^2\rangle$[c] $S=0$	$\langle S^2\rangle$[c] $S=1$
1a	7.94	−104.0	0.999	2.005
2a	8.30	−26.0	1.007	2.006
3a	9.28	−14.4	1.012	2.007
4a	10.72	−4.7	1.531	2.541
5a	12.46	+3.2	2.254	3.254
6a	14.39	+1.7	2.398	3.398
7a	16.44	+0.7	2.423	3.425
8a	18.58	+0.5	2.582	3.587
9a	20.77	+0.7	2.944	3.944
10a	23.01	+1.0	3.364	4.364

[a] Intermetallic distance. [b] Singlet−triplet energy gap. [c] Eigenvalue of the spin operator S^2.

Table 5. Selected Calculated Magnetostructural Data for Model Complexes **1b**−**10b**

complex	r (Å)[a]	J (cm^{-1})[b]	$\langle S^2\rangle$[c] $S=0$	$\langle S^2\rangle$[c] $S=1$
1b	7.94	−104.0	0.999	2.005
2b	10.09	−48.1	1.005	2.007
3b	12.33	−32.1	1.009	2.007
4b	14.62	−10.8	1.460	2.475
5b	16.94	+7.0	2.229	3.227
6b	19.29	+3.9	2.381	3.381
7b	21.64	+1.5	2.394	3.397
8b	24.00	+0.6	2.556	3.542
9b	26.37	+1.0	2.892	3.893
10b	28.75	+3.0	3.303	4.303

[a] Intermetallic distance. [b] Singlet−triplet energy gap. [c] Eigenvalue of the spin operator S^2.

Energy calculations on the two series of C_{2h}-symmetric model complexes **1a**−**10a** and **1b**−**10b** showed a fairly small attenuation of the magnetic coupling with the number of benzenoid repeating units together with a unique wirelike magnetic behavior for the longer members of the series (Figure 5). Thus, the calculated singlet−triplet energy gap decreases almost exponentially for $n = 1-8$, and then it increases smoothly for $n = 9$ and 10 (Tables 4 and 5). Interestingly, the calculations predict a faster exponential decay of the magnetic coupling with the intermetallic distance for **1a**−**8a** than for **1b**−**8b**. The calculated values of the exponential factor are 0.45 and 0.31 Å^{-1}, respectively (solid lines in Figure 5), reflecting thus the relative efficiency of β,β'- over α,α'-disubstituted oligoacene spacers on long-range magnetic coupling, as observed experimentally. In the related series of dicopper(II) metallacyclophanes with oligo-*p*-phenylene spacers, an intermediate exponential decay of the magnetic coupling with an exponential factor of 0.35 Å^{-1} has also been predicted but no similar wirelike magnetic properties have been reported.[12b]

On the other hand, a switch from antiferromagnetic to ferromagnetic coupling is observed along both series of dicopper(II) metallacyclophanes with oligoacene spacers, with a

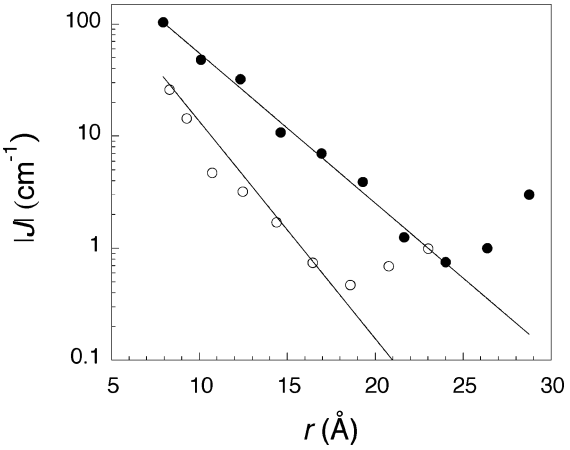

Figure 5. Decay law of the calculated magnetic coupling (on a log scale) with the intermetallic distance for **1a**−**10a** (○) and **1b**−**10b** (●). Solid lines correspond to the best exponential fits (see text).

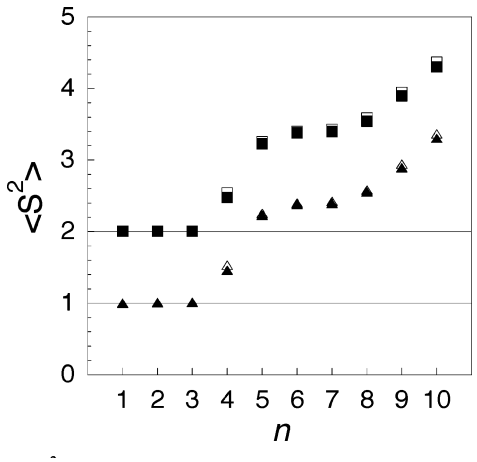

Figure 6. Plot of the calculated $\langle S^2 \rangle$ values for the BS singlet (triangles) and triplet (squares) spin states with the number of repeating units for model complexes **1a**−**10a** (white symbols) and **1b**−**10b** (black symbols). The horizontal lines correspond to the expected eigenvalues for a dicopper(II) complex with either a BS singlet or a triplet spin state.

ground triplet spin state slightly below the excited singlet spin state for $n = 5-10$ (Tables 4 and 5). Notably, the calculations predict a small but nonnegligible ferromagnetic coupling ($J = +3.0$ cm^{-1}) between the two Cu^{II} ions separated by up to 28.8 Å through 2,6-decacenediamidate bridges in **10b**. Hence, it appears that a different mechanism of the electron exchange interaction is operative for the large oligoacene spacers. In both series, a remarkable increase in spin contamination of both singlet and triplet spin states is observed for $n \geq 4$. This is reflected in the calculated eigenvalues of the spin operator S^2 for the BS singlet and triplet spin states of **4a**−**10a** and **4b**−**10b** (Tables 4 and 5), when compared to those expected for a dicopper(II) complex with either a BS singlet or a triplet spin state ($\langle S^2 \rangle = 1$ and 2, respectively) (Figure 6). This situation points out the development of an important polyradical character at the ligand counterparts for $n = 4-10$, as confirmed by the spin density calculations.

Spin Density Analysis: Orbital Mechanism of Magnetic Coupling. Spin densities obtained by NBO analysis on the model complexes **2a** and **3b**, with ideal C_{2h} symmetry (see Computational Details), agree with a spin polarization mechanism through the π-type orbital pathways of the 1,5-naphthalene- and 2,6-anthracenediamidate bridges. This is evidenced by the

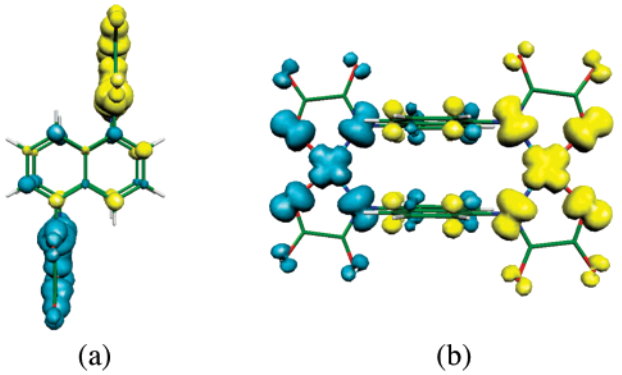

Figure 7. (a) Top and (b) side projection views of the calculated spin density distribution for the ground BS singlet spin configuration of **2a**. Yellow and blue contours represent positive and negative spin densities, respectively. The isodensity surface corresponds to a value of 0.001 e bohr^{-3}.

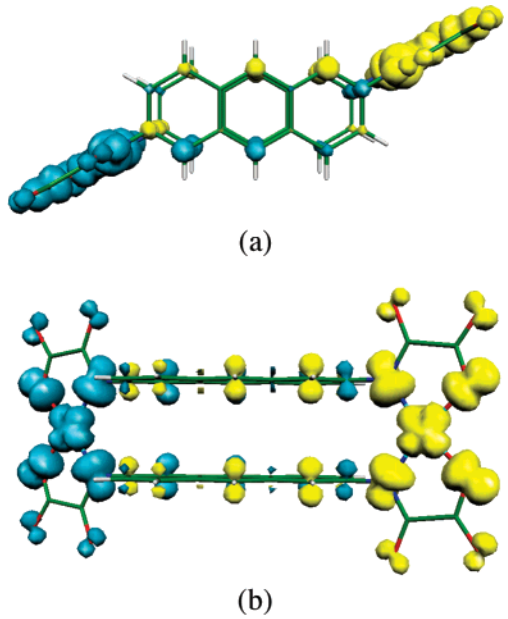

Figure 8. (a) Top and (b) side projection views of the calculated spin density distribution for the ground BS singlet spin configuration of **3b**. Yellow and blue contours represent positive and negative spin densities, respectively. The isodensity surface corresponds to a value of 0.001 e bohr^{-3}.

calculated spin density distribution for the ground BS singlet spin state of **2a** and **3b** (Figures 7 and 8). As expected for a bridging ligand designed with an orthogonal disposition of the aromatic groups with the copper basal planes, there is an extensive delocalization and polarization of the unpaired electrons of the square-planar Cu^{II} ions into the π-conjugated electron system of the aromatic bridges. In this case, the available π orbitals of the aromatic bridges, which are made up of p_z-type orbitals of N and C atoms, largely overlap with the Cu d_{xy} orbitals pointing along the Cu−N and Cu−O bonds because of the strong covalency of the metal−ligand bonds. Thus, the spin densities at the amidate-nitrogen [average values of +0.099 (**2a**) and +0.096 e (**3b**)] and carboxylate-oxygen atoms [average values of +0.096 (**2a**) and +0.099 e (**3b**)] are important and have the same sign as that in the copper atom [average values of +0.559 (**2a**) and +0.561 e (**3b**)], indicating thus that the spin delocalization from the metal toward the donor atoms of the oxamate groups dominates over the spin polarization effects. In contrast, the sign alternation of the spin density at the carbon atoms of the naphthalene and anthracene spacers

Table 6. Selected Calculated Spin Density Data for Model Complexes **1a**−**10a**

	ρ_M (e)[a]		ρ_{MF} (e)[b]		ρ_{LF} (e)[c]	
complex	$S=0$	$S=1$	$S=0$	$S=1$	$S=0$	$S=1$
1a	0.556	0.562	1.006	1.012	0.126	0.028
2a	0.558	0.559	1.005	1.002	0.189	0.093
3a	0.558	0.559	1.004	1.005	0.282	0.125
4a	0.558	0.558	1.004	1.004	1.846	1.867
5a	0.558	0.558	1.002	1.002	3.139	3.138
6a	0.557	0.557	1.000	1.000	3.659	3.659
7a	0.556	0.556	0.999	0.999	4.070	4.071
8a	0.555	0.555	0.997	0.997	4.673	4.678
9a	0.553	0.553	0.995	0.995	5.520	5.519
10a	0.552	0.552	0.992	0.992	6.394	6.396

[a] Metal atomic spin density. [b] Metal fragment spin density defined as the sum of the atomic spin densities (in absolute values) for each metal plus two oxamate binding groups. [c] Ligand fragment spin density defined as the sum of the atomic spin densities (in absolute values) for each oligoacene spacer group.

Table 7. Selected Calculated Spin Density Data for Model Complexes **1b**−**10b**

	ρ_M (e)[a]		ρ_{MF} (e)[b]		ρ_{LF} (e)[c]	
complex	$S=0$	$S=1$	$S=0$	$S=1$	$S=0$	$S=1$
1b	0.556	0.562	1.006	1.012	0.126	0.028
2b	0.561	0.562	1.009	1.011	0.161	0.056
3b	0.560	0.561	1.008	1.010	0.244	0.090
4b	0.560	0.560	1.006	1.007	1.719	1.754
5b	0.559	0.559	1.001	1.001	3.106	3.109
6b	0.557	0.557	0.996	0.995	3.629	3.628
7b	0.555	0.555	0.991	0.991	4.015	4.019
8b	0.553	0.553	0.987	0.986	4.595	4.710
9b	0.551	0.551	0.982	0.982	5.423	5.423
10b	0.545	0.549	0.974	0.973	6.281	6.279

[a] Metal atomic spin density. [b] Metal fragment spin density defined as the sum of the atomic spin densities (in absolute values) for each metal plus two oxamate binding groups. [c] Ligand fragment spin density defined as the sum of the atomic spin densities (in absolute values) for each oligoacene spacer group.

agrees with a spin polarization by the amidate-nitrogen donor atoms, leading thus to significant spin densities of opposite sign at the carbon atoms of the terminal benzene rings to which they are directly attached [average values of −0.011 (**2a**) and −0.010 (**3b**) e]. Because of the peculiar topology of these bridges with an even number of carbon atoms between the two amidate-nitrogen atoms (1,5- and 2,6-substitution patterns), the spin densities at the two copper atoms have opposite signs and then a net antiferromagnetic exchange interaction results for both **2a** and **3b**.

Spin densities obtained by NBO analysis on the two series of C_{2h}-symmetric model complexes **1a**−**10a** and **1b**−**10b** conform with a gradual change from a closed-shell to an open-shell diradical formulation for the oligoacenebis(oxamate) bridging ligands. A quantitative description of the spin redistribution that occurs upon electron exchange along these two series, particularly within the metallacyclophane core structure, can be obtained from the calculated spin densities for the metal (ρ_{MF}) and the ligand (ρ_{LF}) fragments, which are defined as the sum of the atomic spin densities (in absolute values) for each metal plus two oxamate binding groups on the one hand and for each oligoacene spacer group at the other hand (Tables 6 and 7). Whereas the spin population at the metal atoms (ρ_M) and the metal-bis(oxamate) fragments (ρ_{MF}) are roughly constant along the two series, a dramatic increase in the spin population at the carbon atoms of the oligoacene spacers (ρ_{LF}) occurs in

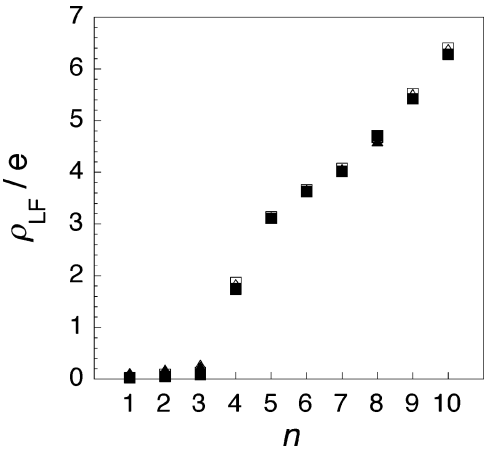

Figure 9. Plot of the calculated ligand fragment spin density for the BS singlet (triangles) and triplet (squares) spin states with the number of repeating units for model complexes **1a**−**10a** (white symbols) and **1b**−**10b** (black symbols).

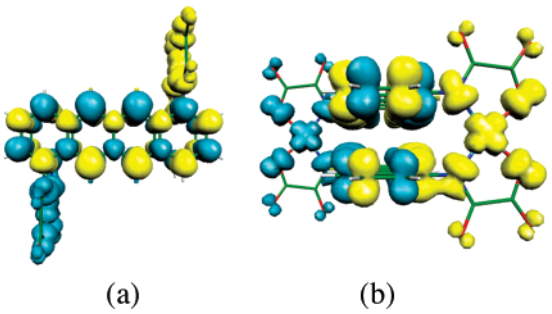

Figure 10. (a) Top and (b) side projection views of the calculated spin density distribution for the ground BS singlet spin configuration of **4a**. Yellow and blue contours represent positive and negative spin densities, respectively. The isodensity surface corresponds to a value of 0.001 e bohr^{-3}.

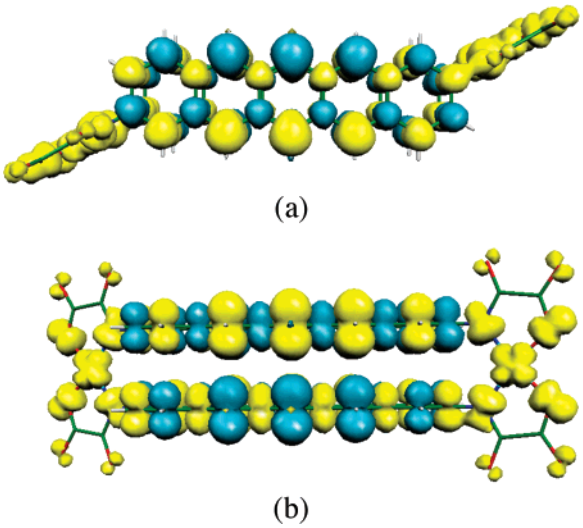

Figure 11. (a) Top and (b) side projection views of the calculated spin density distribution for the ground triplet spin configuration of **5b**. Yellow and blue contours represent positive and negative spin densities, respectively. The isodensity surface corresponds to a value of 0.001 e bohr^{-3}.

both the BS singlet and the triplet spin states for $n \geq 4$ (Figure 9). This is exemplified by the calculated spin density distribution for the ground BS singlet and triplet spin state of **4a** and **5b**, respectively (Figures 10 and 11), which shows a large amount of spin density of global opposite sign delocalized along each of the two oligoacetylene ribbons of the tetracene and pentacene

Scheme 2. Dual Exchange Coupling Mechanism in the Dinuclear Copper(II) Metallacyclophanes with α,α′- and β,β′-Disubstituted Oligoacene Spacers[a]

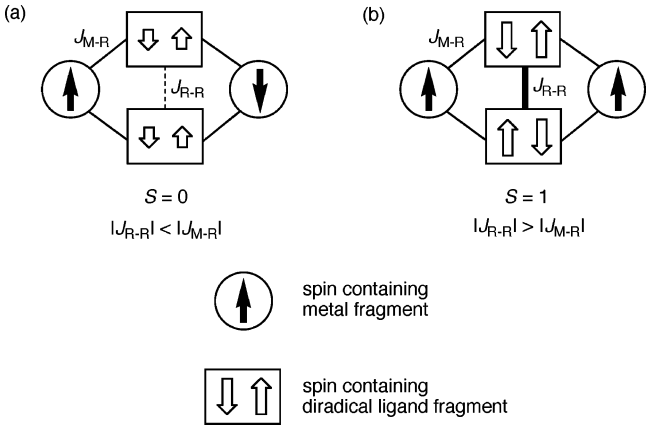

[a] (a) Through-bond metal-radical and (b) through-space radical−radical antiferromagnetic (AF) coupling regimes.

spacers and partially polarized at the carbon atoms connecting the two oligoacetylene halves. Such oligoacenes beyond tetracene would then behave as two oligoacetylene monoradicals connected by C−C bonds with a singlet diradical ground spin state. A similar phenomenon has been recently reported for the oligoacene molecules themselves, but the transition toward the open-shell singlet diradical ground state occurs beyond octacene.[14a] This difference is a consequence of the metal-promoted through-bond spin polarization operating in the dicopper(II) metallacyclophanes with α,α′- and β,β′-disubstituted oligoacene spacers.

The spin densities on the model complexes **1a**−**10a** and **1b**−**10b** also reflect the increased participation of direct C−C exchange interactions between the two facing oligoacene spacers that occurs in both the BS singlet and the triplet spin states for $n \geq 4$. For instance, this is illustrated in the calculated spin density distributions for the ground BS singlet and triplet spin states of **4a** and **5b**, respectively (Figures 10b and 11b), which show a sign alternation of the spin density at the directly opposed carbon atoms of the two spacers within the metallacyclophane cores. This situation clearly contrasts with that found for the ground BS singlet spin state of **2a** and **3b** (Figures 7b and 8b), which shows spin densities of the same sign at the equivalent carbon atoms of the two facing naphthalene and anthracene spacers within the metallacyclophane core. The observed dual regime for the magnetic exchange coupling mechanism in the model complexes **1a**−**10a** and **1b**−**10b** is illustrated in Scheme 2. In this case, the spin density developed at the short oligoacene spacers as a result of the spin polarization mechanism has been assigned to an incipient diradical ligand formation by analogy to what effectively occurs for the long oligoacene spacers. The through-bond metal-radical antiferromagnetic coupling (J_{M-R}) dominates over the through-space radical−radical one (J_{R-R}) for the shortest members of the series with $n = 1-4$; hence, a net metal−metal antiferromagnetic coupling ($J < 0$) results with a ground singlet spin state (Scheme 2a). Instead, the through-space radical−radical antiferromagnetic coupling (J_{R-R}) dominates over the through-bond metal-radical one (J_{M-R}) for the longest members of the series with $n \geq 5$, and then a net metal−metal ferromagnetic coupling ($J > 0$) results with a ground triplet spin state (Scheme 2b). This picture is reminiscent of a spin frustrated system with competitive through-bond and through-space antiferromagnetic couplings between the local spins centered on the metal and the diradical ligand fragments. Hence, the overall antiferromagnetic $\pi-\pi$ coupling between the two diradical ligands is ultimately responsible for the variation in the spin multiplicity of the ground state for the longer members of the series.[15]

3. Conclusions

Molecular and electronic structure calculations on the dicopper(II) metallacyclophanes with α,α′- and β,β′-disubstituted oligoacenebis(oxamate) bridging ligands identify the bridging topology as the main factor in controlling the magnitude of the exchange interaction between the two metal centers, as confirmed experimentally for the short oligoacene spacers. In fact, a moderately strong intramolecular magnetic coupling between the two Cu^{II} ions separated by a relatively large intermetallic distance has been observed due to spin polarization effects across the 1,5-naphthalene and 2,6-anthracene spacers. More importantly, the calculations predict a wirelike magnetic coupling between two Cu^{II} ions with the increasing intermetallic distance for octacene through decacene spacers. This unprecedented magnetic behavior arises from the intrinsic electroactive properties of the large oligoacene spacers, which have a singlet diradical character with important spin delocalization and spin polarization within each of the two oligoacetylene ribbons to which the metal centers are attached. In contrast to conventional charge transport-based molecular wires, these so-called "magnetic molecular wires" may offer a new design concept for the transfer of information over long distances based on purely electron exchange interactions and involving no current flow. This leads our current synthetic efforts to obtain dicopper(II) metallacyclophanes with large oligoacene spacers as potential candidates to nanometer-scale electronic devices in the emerging field of molecular spintronics.

4. Experimental Section

Materials. All chemicals were of reagent grade quality, and they were purchased from commercial sources and used as received. 2,6-Anthracenediamine was prepared by reduction of the commercially available 2,6-anthraquinone with zinc, as reported in the literature.[16]

H_2Et_2-1,5-naba: Ethyl oxalyl chloride ester (7.0 mL, 60 mmol) was added all at once to a solution of 1,5-naphthalenediamine (5.75 g, 30 mmol) in THF (250 mL) under vigorous stirring at 0 °C in an ice bath. The reaction mixture was charged with triethylamine (2.8 mL, 20 mmol), and it was heated to reflux for 1 h. The light gray solid was collected by filtration after cooling, washed thoroughly with water to eliminate the precipitate of Et_3NHCl, and dried under vacuum (9.25 g, 85% yield). Anal. Calcd for $C_{18}H_{18}N_2O_6$ (358): C, 60.34; H, 5.03; N, 7.82. Found: C, 60.77; H, 5.17; N, 7.52. ^{1}H NMR (C_2D_6SO): δ 1.35 (t, $J = 7.2$ Hz, 6 H, 2 CH_3), 4.37 (q, $J = 7.2$ Hz, 4 H, 2 CH_2O), 7.57 (dd, $J = 7.2$ and 2.8 Hz, 2−H, 4−H, and 8−H of $C_{10}H_6N_2$), 7.59 (t, $J = 7.2$ Hz, 2−H, 3−H, and 7−H of $C_{10}H_6N_2$), 7.88 (dd, $J = 6.3$ and 2.8 Hz, 2−H, 2−H, and 6−H of $C_{10}H_6N_2$), 10.98 (s, 2 H, 2 NH). IR (KBr, cm^{-1}): 3206 (NH), 1738, 1686 (CO).

H_2Et_2-2,6-anba. Ethyl oxalyl chloride ester (2.3 mL, 20 mmol) was added all at once to a solution of 2,6-anthracenediamine (2.08 g, 10

(15) Preliminary DFT energy calculations on the related dinuclear copper(II) model complexes with single α,α′- and β,β′-disubstituted oligoacenebis(oxamate) bridging ligands show a singlet spin ground state lying well below the triplet excited state in all cases. In both series, the calculated $-J$ value decreases with the number of benzenoid repeating units for $n = 1-3$, and then it increases continuously for $n = 4-10$ as a result of the open-shell singlet diradical character of the oligoacene spacers (data reported elsewhere).

(16) Rabjohns, M. A.; Hodge, P.; Lovell, P. A. *Polymer* **1997**, *38*, 3395.

mmol) in THF (250 mL) under vigorous stirring at 0 °C in an ice bath. The reaction mixture was charged with triethylamine (2.8 mL, 20 mmol), and it was heated to reflux for 3 h under argon. The light yellow solid was collected by filtration after cooling, washed thoroughly with water to eliminate the precipitate of Et_3NHCl, and dried under vacuum (3.3 g, 80% yield). Anal. Calcd for $C_{22}H_{20}N_2O_6$ (408): C, 64.71; H, 4.90; N, 6.86. Found: C, 65.03; H, 4.78; N, 6.98. ^{1}H NMR (C_2D_6SO): δ 1.35 (t, J = 7.2 Hz, 6−H, 2 CH_3), 4.35 (q, J = 7.2 Hz, 4−H, 2 CH_2O), 7.78 (d, J = 7.7 Hz, 2−H, 3−H, and 7−H of $C_{14}H_8N_2$), 8.06 (d, J = 9.2 Hz, 2−H, 4−H, and 8−H of $C_{14}H_8N_2$), 8.47 (s, 2−H, 1−H, and 5−H of $C_{14}H_8N_2$), 8.57 (s, 2−H, 9−H, and 10−H of $C_{14}H_8N_2$), 11.03 (s, 2−H, 2−NH). IR (KBr, cm^{-1}): 3226 (NH), 1735, 1692, 1685 (CO).

$Li_4$2a·12H_2O. A solution of $LiOH·H_2O$ (0.84 g, 20.0 mmol) in water (25 mL) was added to a suspension of H_2Et_2-1,5-naba (1.79 g, 5.0 mmol) in methanol (25 mL). A solution of $Cu(NO_3)_2·3H_2O$ (1.20 g, 5.0 mmol) in water (25 mL) was added dropwise after stirring for 15 min at room temperature. The resulting deep brown solution was then filtered, and the solvent was reduced under vacuum until a dark brown solid appeared. The solid was collected by filtration, washed with acetone and diethyl ether, and dried under vacuum (1.5 g, 60% yield). Anal. Calcd for $C_{28}H_{36}Cu_2Li_4N_4O_{24}$ (967): C, 31.72; H, 3.69; N, 5.35. Found: C, 31.61; H, 3.22; N, 5.78. IR (KBr, cm^{-1}): 3412 (OH), 1615, 1607 (CO).

(Ph_4P)$_4$2a·8H_2O. A solution of $AgNO_3$ (0.68 g, 4.0 mmol) in water (10 mL) was added to a solution of Li_4**2a**·12H_2O (0.97 g, 1.0 mmol) in water (50 mL). The brown solid which appeared was collected by filtration after stirring for 15 min at room temperature. A suspension of this solid in water (50 mL) was charged with a solution of Ph_4PCl (1.50 g, 4.0 mmol) in water (10 mL). The reaction mixture was further stirred for 30 min under gentle warming and then filtered to remove the solid AgCl. Large dark brown prisms suitable for X-ray diffraction were obtained by slow evaporation of the filtered solution in air at room temperature (1.8 g, 80% yield). Anal. Calcd for $C_{124}H_{108}Cu_2N_4O_{20}P_4$ (2223): C, 65.89; H, 4.85; N, 2.52. Found: C, 66.57; H, 4.67, N 2.67. IR (KBr, cm^{-1}): 3414 (OH), 1617, 1606 (CO).

$Li_4$3b·12H_2O. A solution of $LiOH·H_2O$ (0.51 g, 12.0 mmol) in water (25 mL) was added to a suspension of H_2Et_2-2,6-anba (1.22 g, 3.0 mmol) in methanol (25 mL). A solution of $Cu(NO_3)_2·3H_2O$ (0.72 g, 3.0 mmol) in water (25 mL) was added dropwise after stirring for 15 min at room temperature. The resulting deep green solution was then filtered, and the solvent was reduced under vacuum until a dark green solid appeared. The solid was collected by filtration, washed with acetone and diethyl ether, and dried under vacuum (0.7 g, 40% yield). Anal. Calcd for $C_{36}H_{40}Cu_2Li_4N_4O_{24}$ (1067): C, 40.49; H, 3.75; N, 5.25. Found: C, 40.29; H, 3.72; N, 5.40. IR (KBr, cm^{-1}): 3412 (OH), 1615, 1607 (CO).

(Ph_4P)$_4$3b·4H_2O. A solution of Ph_4PCl (0.75 g, 2.0 mmol) dissolved in water (10 mL) was added to a solution of Li_4**3b**·12H_2O (0.53 g, 0.5 mmol) in water (15 mL). The green solid which appeared was collected by filtration and dried under vacuum (0.8 g, 70% yield). Anal. Calcd for $C_{132}H_{104}Cu_2N_4O_{16}P_4$ (2251): C, 70.37; H, 4.62; N, 2.49. Found: C, 70.11; H, 4.02, N 2.54. IR (KBr, cm^{-1}) 3425 (OH), 1633, 1599 (CO).

Physical Techniques. ^{1}H NMR spectra were recorded at room temperature on a Bruker AC 200 (200.1 MHz) spectrometer. C_2D_6SO was used as solvent and internal standard (δ 2.50). IR spectra were recorded on a Perkin-Elmer 882 spectrophotometer as KBr pellets. Elemental analyses (C, H, N) were performed by the Microanalytical Service of the Universidad Autónoma de Madrid (Spain).

Crystal Structure Data Collection and Refinement. The structure of (Ph_4P)$_4$**2a**·8H_2O was solved by direct methods and refined with the full-matrix least-squares technique on F^2 using the SHELXS-97 and SHELXL-97 programs.[17a] Data collection and data reduction were done with the COLLECT[17b] and EVALCCD[17c] programs. Empirical absorption corrections were carried out using SADABS[17d] for all compounds. All calculations for data reduction, structure solution, and refinement were done according to standard procedures (WINGX).[17e] The final geometrical calculations and the graphical manipulations were carried out with PARST97[17f] and CrystalMaker[17g] programs, respectively. The hydrogen atoms from the organic ligands were calculated and refined with isotropic thermal parameters, while those from the water molecules were neither found nor calculated.

Magnetic Measurements. Variable-temperature (4.0−300 K) magnetic susceptibility measurements under an applied magnetic field of 1.0 T were carried out on powdered samples with a SQUID magnetometer. The experimental data were corrected for the diamagnetism of the constituent atoms and the sample holder.

5. Computational Details

Electronic structure calculations were carried out with the hybrid density functional B3LYP method[18] combined with the broken-symmetry (BS) approach[19] by using the Gaussian-03 program[20] and the triple-ζ (TZV) basis set proposed by Ahlrichs and co-workers.[21] A quadratic convergence method was employed in the SCF process. The atomic spin densities were obtained from Natural Bond Orbital (NBO) analysis.[22] Molecular geometries of model complexes **1a**−**10a** and **1b**−**10b** were not optimized, but their structural parameters were taken from the crystal structure of **2a** (ϕ = 90° and τ = 0°), with imposed intra- and inter-ring C−C distances of 1.415 and 3.455 Å, respectively. The C_{2h} symmetry constraint was considered in all the calculations. The energy values of the BS singlet and triplet spin states for **1a**−**3a** and **1b**−**3b** were obtained from a wave function corresponding to two local spins with opposite or identical signs, respectively, centered on the metal ions. These wave functions were also found for **4a**−**10a** and **4b**−**10b**; however, a stability test applied to them revealed the presence of more stable solutions with a nonnegligible polyradical contribution at the ligand counterparts.

Acknowledgment. This work was supported by the MEC (Spain) (Projects CTQU2004-03633, CTQ2005-08123-C02-02/BQU and MAT2004-03112), the Catalan Government (2005SGR-00036), and the European Union (HRM Project Quantum Effects in Molecular Nanomagnets, QuEMolNa MRTN-CT-2003-504880). E.P. thanks the MEC for a grant. We are especially thankful to Dr G. Blay and Dr I. Fernández (Universitat de València) for unselfish help in the preparation and characterization of the ligands and to Dr S. Stiriba (Universitat de València) and Dr X. Ottenwaelder (Concordia University) for very stimulating talks and continuous interest in this work.

Supporting Information Available: Crystallographic data (excluding structure factors) for the structure reported in this paper have been deposited with the Cambridge Crystallographic

(17) (a) Sheldrick, G. M. *SHELX97*, *Programs for Crystal Structure Analysis* (release 97-2); Institüt für Anorganische Chemie der Universität: Göttingen, Germany, 1998. (b) Hooft, R. W. W. *COLLECT*; Nonius BV: Delft, The Netherlands, 1999. (c) Duisenberg, A. J. M.; Kroon-Batenburg, L. M. J.; Schreurs, A. M. M. *J. Appl. Crystallogr.* **2003**, *36*, 220 (EVALCCD). (d) *SADABS*, version 2.03; Bruker AXS Inc.: Madison, WI, 2000. (e) Farrugia, L. J. *J. Appl. Crystallogr.* **1999**, *32*, 837 (*WINGX*). (f) Nardelli, M. *J. Appl. Crystallogr.* **1995**, *28*, 659. (g) Palmer, D. *CrystalMaker*, version 7.2; Cambridge University Technical Services: Cambridge, U.K., 2007.
(18) Becke, A. D. *J. Chem. Phys.* **1993**, *98*, 5648.
(19) (a) Ruiz, E.; Alemany, P.; Alvarez, S.; Cano, J. *J. Am. Chem. Soc.* **1997**, *119*, 1297. (b) Ruiz, E.; Cano, J.; Alvarez, S.; Alemany, P. *J. Am. Chem. Soc.* **1998**, *120*, 11122. (c) Ruiz, E.; Cano, J.; Alvarez, S.; Alemany, P. *J. Comput. Chem.* **1999**, *20*, 1391. (d) Ruiz, E.; Rodriguez-Fortea, A.; Cano, J.; Alvarez, S.; Alemany, P. *J. Comput. Chem.* **2003**, *24*, 982. (e) Ruiz, E.; Polo, V.; Cano, J.; Alvarez, S. *J. Chem. Phys.* **2005**, *123*, 164110.
(20) Frisch, M. J. et al. *Gaussian 03*, revision C.02; Gaussian, Inc.: Wallingford, CT, 2004.
(21) (a) Schaefer, A.; Horn, H.; Ahlrichs, R. *J. Chem. Phys.* **1992**, *97*, 2571. (b) Schaefer, A.; Huber, C.; Ahlrichs, R. *J. Chem. Phys.* **1994**, *100*, 5829.
(22) (a) Carpenter, J. E.; Weinhold, F. *J. Mol. Struct.* **1988**, *169*, 41. (b) Reed, A. E.; Curtis, L. A.; Weinhold, F. *Chem. Rev.* **1988**, *88*, 899. (c) Weinhold, F.; Carpenter, J. E. *The Structure of Small Molecules and Ions*; Plenum: 1988; p 227.

Data Centre as supplementary publication no. CCDC−624489. Copies of the data can be obtained free of charge on application to CCDC, 12 Union Road, Cambridge CB21EZ, UK (fax: (+44) 1223−336-033; e-mail: deposit@ccdc.cam.ac.uk). Selected magnetostructural data for dicopper(II) metallaazacyclophanes with extended aromatic bridges (Table S1). Absolute energies (Tables S2 and S3) and geometries (Tables S4−S23) for model compounds **1a**−**10a** and **1b**−**10b**. Complete ref 20. Crystal packing view of $(Ph_4P)_4$**2a**$\cdot 8H_2O$. This material is available free of charge via the Internet at http://pubs.acs.org.

JA0747066